The effect of porosity on thermal properties: towards a threshold of particle contact in sintered stainless steel

2005 J. Phys.: Condens. Matter 17 1239

(http://iopscience.iop.org/0953-8984/17/7/016)

INSTITUTE OF PHYSICS PUBLISHING JOURNAL OF PHYSICS: CONDENSED MATTER

J. Phys.: Condens. Matter **17** (2005) 1239–1249 doi:10.1088/0953-8984/17/7/016

The effect of porosity on thermal properties: towards a threshold of particle contact in sintered stainless steel

W M Lima, V Biondo, W R Weinand, E S Nogueira, A N Medina, M L Baesso and A C Bento[1]

Departamento de Física, Universidade Estadual de Maringá, Avenida Colombo, 5790, Maringá-PR-Brazil, 87020-900, Brazil

E-mail: acbento@uem.br

Received 10 November 2004, in final form 18 January 2005
Published 4 February 2005
Online at stacks.iop.org/JPhysCM/17/1239

Abstract

The thermal diffusivity and thermal conductivity of sintered stainless steel AISI 316L, obtained as a function of compacting pressures, are provided. The thermal parameters were measured by photoacoustic and thermal relaxation methods. The results suggest a strong correlation with the particles' effective area of contact whilst an S-shape behaviour shows striking increasing physical properties for uniaxial pressure close to 490 MPa. A limiting density of particle contact exists over a *percolation threshold* when the porosity is reduced to less than 8%.

1. Introduction

Stainless steel (SS) produced via powder metallurgy (P/M) is known to have different physical properties when compared to that produced by conventional techniques. This material presents intrinsic porosity for use as a functional gradient in filtering processes. Actually the degree of compacting pressure used during the material preparation defines its characteristics. Moreover, a precise evaluation of the influence of the resulting porosity level and the fraction of interconnected pores on the material properties is a difficult task [1, 2]. Since the heat diffusion process is one of the most important properties that may be used to evaluate the structure of this material, the measurement of thermal conductivity, thermal diffusivity and specific heat may provide information on the sample preparation conditions and the figure of merit of the obtained material.

Heat diffusion processes of materials containing several phases, impurities, and porosity cannot be treated as those of conventional amorphous or crystalline solids. Final measured properties, such as thermal conductivity, have an effective value with a contribution from different heat diffusion mechanisms [3–5]. Previous works have investigated the correlation

[1] Author to whom any correspondence should be addressed.

between microstructure and thermal conductivity of porous materials, taking into account the effective value for this parameter in terms of the fraction volume occupied by the grain-boundary phase [5–8]. These descriptions predict that conducting materials in high porosity regime present a exponential decrease in thermal conductivity values in proportion to an increase in porosity degree [9]: if the porosity is a small part of the sample's fraction volume, the behaviour is almost linear [2]. In both cases, the phenomenological constants related to the material composition, porous geometry and distribution have to be taken into account. On the other hand, if the material is designed to have a small amount of a second phase instead of pores, the effective thermal properties may present neither an exponential behaviour nor a linear one, similar to that reported in polymer composites filled with carbon conducting particles [6]. In this case, after a certain amount of carbon has been exceeded, the thermal conductivity presents a transition with a large increase in value. Walther and co-workers [4] associated this fact with an additional transport mechanism in a sample governed by phonons and electronic contributions, generated after a percolation threshold by exceeding electrically conductive clusters formed in the disordered matrix.

Conventional determination of thermal properties, such as thermal diffusivity and thermal conductivity of matter, demands indirect methods or comparative probes, with some inaccuracy in experimental results. Nowadays, such properties can be accurately determined by modern photothermal methods [10–13] that use lasers as the remote heating source. One of these methods is the open photoacoustic cell (OPC) used to measure the thermal diffusivity of resins, polymers, metal foils and semiconductors, such as porous silicon [14–16]. The non-adiabatic thermal relaxation calorimetric method (NATRC) may be applied for specific heat assessment [17, 18]. The advantage of these methods is that they are non-destructive, allowing the same sample to be later inspected by other techniques. Thermal conductivity may be thus calculated by thermal diffusivity, mass density and specific heat.

The aim of our current research is to evaluate the effects of porosity on the thermal properties of sintered SS 316L by the photothermal method.

2. Theory

2.1. Open photoacoustic cell—OPC

The OPC technique consists of a commercial electret's microphone, in which the microphone chamber functions as a photoacoustic cell. Figures 1(a) and (b) show the apparatus used in the experiments. The sample is placed directly on top of the microphone to seal the chamber. If a modulated light beam is shining on the sample surface, a periodic heat is generated which, in turn, induces a pressure variation inside the chamber. The chamber pressure may be calculated by solving a set of thermal diffusion equations with appropriate boundary conditions [19], such as no lateral heat losses in the cell and strong absorbing material, with $\beta(\lambda)l_s \gg 1$, in which $\beta(\lambda)$ is the optical absorption coefficient and l_s the sample thickness. In this framework, the pressure inside the cell is given as follows [14]:

$$P(f) = \frac{\gamma P_0 I_0 (\alpha_s \alpha_g)^{\frac{1}{2}}}{\pi T_0 l_g k_S} e^{j(\omega t - \frac{\pi}{2})} \frac{e^{-l_s\sqrt{\frac{\pi f}{\alpha_s}}}}{f}. \tag{1}$$

Thermophysics and geometric parameters are defined as: I_0 = light intensity (W m^{-2}), $\gamma = c_p/c_v$ is the specific heat ratios (p is the pressure and v is the volume), P_0 = room pressure (atm), $T_0 \equiv$ room temperature (°C), k_s = thermal conductivity (W m^{-1} K^{-1}), σ_s = thermal wavevector, $\omega(=2\pi f)$ = angular frequency (rad s^{-1}) and α = thermal diffusivity (m^2 s^{-1}) (s: sample and g: gas). In the case of an opaque and thermally thick sample (thickness greater

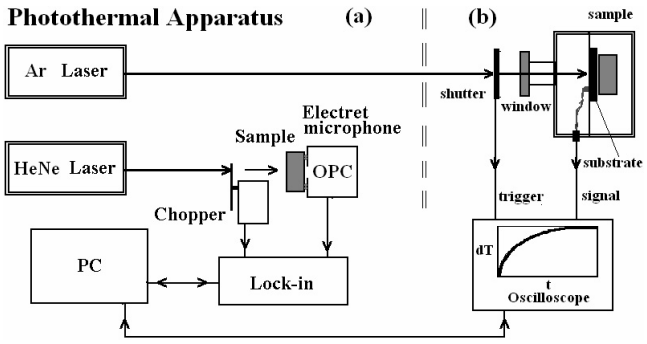

Figure 1. Experimental arrangements for thermal property measurements: (a) thermal diffusivity and (b) specific heat.

than thermal wavelength, $l \gg \mu = \sqrt{\alpha_s/\pi f}$), one may estimate that the chamber pressure varies as an exponential function of modulation frequency. The photoacoustic signal is given as

$$P(f) \propto S(f) \cong \frac{1}{f} e^{-b\sqrt{f}}. \tag{2}$$

Parameter b is related to the thermal diffusivity by $b = l_s\sqrt{\pi\alpha_s}$; if the sample thickness is known, the thermal diffusivity will be obtained by fitting the experimental data to the above equation. The thermal conductivity k_s is then calculated from the thermal diffusivity, $\alpha = k_s/\rho c_p$, since the mass density and specific heat are already known.

2.2. Non-adiabatic thermal relaxation calorimetric—NATRC

NATRC is a transient method that monitors the time evolution of the temperature of a substrate that supports the slab; figure 1(b). The total absorbed power P is given by [17, 18]

$$P(t) = C\frac{d}{dt}\Delta T + K\Delta T, \tag{3}$$

in which C is the system heat capacity, K is the effective thermal conductance of the system (substrate + sample) and ΔT is the difference between the temperature of the system and the thermal reservoir. In the steady state condition, the power is $P \sim K\Delta T_{max}$. If the power is switched off, the transient solution is $\Delta T(t) = \Delta T_{max}\exp(-t/\tau)$, in which τ gives the relaxation time for power losses from the whole system. By monitoring the time evolution of temperature rise and fall, the sample's specific heat may be determined by fitting τ and ΔT_{max}. The specific heat of the sample is related to these parameters from $\tau = (C\Delta T_{max})/P$, with $c_p = (C - C_{substrate})\ m^{-1}$, with C as the system heat capacity and P the light power. $C_{substrate}$ should be known in advance and is obtained in the same way by fitting τ and ΔT_{max}.

3. Experimental details

Samples were prepared with commercial powder SS AISI 316L (Hŏgan ăs, Sweden); the particles' size is smaller than 37 μm. The chemical composition of the standard AISI 316L is [65.14% Fe + 16.10% Cr + 13.55% Ni + 2.24% Mo + 2.00% Mn + 0.87% Si + 0.045% P + 0.03% S + 0.021% C] and this is the same for both the powder and the reference sample, an SS foil [1]. The uniaxial compacting pressures varied between 300 and 700 MPa

(1 MPa $= 10^6$ N m^{-2}), at room temperature, in a rigid matrix, which provided samples of 40×10^{-3} m diameter and 2×10^{-3} m thickness. Four samples were produced for each pressure. Sintering was done under vacuum atmosphere (10^{-4} Torr), at 1150 °C, for 30 min. This set of samples was also characterized according to the Standard ISO 2738, in which the porosity was related to the relative density of materials and its evolution was evaluated by scanning electron microscopy (SEM). For thermal diffusivity measurements, each disc was split into smaller parts (replicates), and measurements could be repeated four times. The replicates were cut into discs with 10^{-2} m diameter and 500 μm thicknesses. For thermal diffusivity measurement, a 10 mW He–Ne laser (Uniphase, model 1135P), operating at 632.8 nm, was used. Light modulation frequency was employed by a mechanical chopper (SRS, model 540). The microphone voltage output was measured by a lock-in amplifier (EG&G, model 5110).

Specific heat measurements were made with a home-made NATRC setup. A copper thermal reservoir (25×10^{-3} m diameter), with two thin copper wires (200 μm) holding the silver substrate ($8.5 \times 8.5 \times 0.15$) $\times 10^{-3}$ m, was used in the device. The system was fixed in an external cup with an optical window (12×10^{-3} m in diameter), which allowed the light to reach the substrate. The sample was tightly held at the substrate surface by a very thin coupling glued layer. An argon ion laser (20 mW) induced heating of the sample. The temperature rise was monitored by a differential thermocouple in contact with the substrate, which fed the signal from a microvoltmeter (Keithley 155) into a digital storage oscilloscope (HP 5460).

4. Results and discussion

Table 1 summarizes the values of the sintered stainless steel parameters measured in this research. Values of ρ, c_p and α were measured regardless of the four replicate samples and the average values were taken into account to obtain k. Since errors in this table are the highest deviation found after measuring the specific property of the replicates, they may be considered the representative errors for these properties. The last line of table 1 refers to the measured properties for stainless steel (AISI 316L) obtained by conventional techniques. These properties were taken as standards to have an approach for the limiting case in which the pressure was higher than 700 MPa. The upper limit will be nil porosity ($p = 0\%$) when the pressure is infinite ($P = \infty$). In the case of this particular sample, the value calculated for the thermal conductivity, for instance, $k \sim 0.139 \times 10^2$ W m^{-1} K^{-1}, agreed with that reported in the literature [20].

Figure 2 shows the porosity (upper frame) and density (lower frame) as a function of compacting pressure. At first glance, it may be observed that a non-linear behaviour exists and that both curves tend towards saturation at high pressures ($P > 500$ MPa). Since the porosity decreases as the density increases, the ideal threshold for porosity and density for particle sizes ($\leqslant 37$ μm) is obtained by a pressure close to 700 MPa. On the other hand, it should be noted that both curves present a transition region between 450 and 550 MPa. In fact, if one uses a standard Boltzmann function (or 'S-shaped' curve), both results form a sigmoid curve. The typical 'S-shaped' function may be written as $Bz(P) = \{F_s + [I_s - F_s]/[1 + \exp((P - H_s)/W)]\}$, in which P is the variable (in figure 2, it is the pressure P in MPa) and the other variables are parameters related to the initial saturation (I_s), final saturation (F_s), half excursion (H_s), and finally, the width of the transition region (W). Furthermore, if the second derivative of the fitted S-curves is carried out, then a transition pressure will be found at the inflection point of the two curves. Table 2 shows the results. The transition point was obtained close to 496 MPa corresponding to a density of $\rho \approx 7.1 \times 10^3$ kg m^{-3}. In the case of porosity, the transition was found close to 495 MPa, with porosity close to $p \approx 10.5\%$.

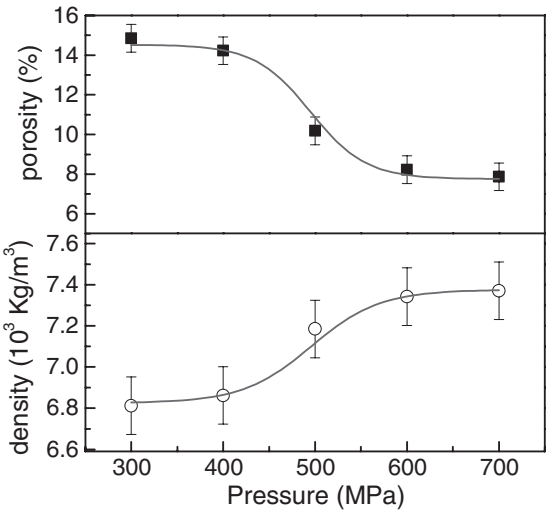

Figure 2. Compacting pressure effects in the sintered SS AISI 316L: (■)—porosity and (○)—density.

Table 1. Results of thermal properties of sintered SS samples.

P (MPa)	ρ (10^3 kg m^{-3}) ± 0.02	p (%)	c_p[a] (10^3 J kg^{-1} K^{-1}) ± 0.01	α[b] (10^{-4} m^2 s^{-1}) ± 0.002	k[c] (10^2 W m^{-1} K^{-1}) ± 0.008
300	6.81	14.8	0.49	0.021	0.069
400	6.86	14.2	0.50	0.020	0.068
500	7.18	10.2	0.48	0.020	0.069
600	7.34	8.2	0.49	0.022	0.080
700	7.37	7.9	0.48	0.032	0.115
$(P \to \infty)$[d]	8.00	$(p \to 0)$	0.50	0.035	0.139

[a] Obtained from NATRC method.
[b] Obtained from OPC measurements.
[c] Calculated from $k = (\alpha \rho c_p)$.
[d] Reference sample AISI 316L foil with the same chemical composition as the powder.

Table 2. Boltzmann analysis of density (ρ) and porosity (p%).

Boltzmann parameters	Density curve	Porosity curve
I_s	$(6.8 \pm 0.2) \times 10^3$ kg m^{-3}	(14.5 ± 0.6)%
F_s	$(7.4 \pm 0.1) \times 10^3$ kg m^{-3}	(7.8 ± 0.6)%
H_s (pressure)	(496 ± 48) MPa	(495 ± 4) MPa
W	(38 ± 64) MPa	(30 ± 27) MPa

Density has a very important role in sintered materials, since it characterizes the level of porosity. This parameter may affect the permeability, and therefore it drives the thermal diffusivity and the thermal conductivity values. In fact, if the compacting pressure increases, the free zones of particle contact will be reduced and the material density highly increases. In this research, the density corresponds to about 92% of the theoretical density of SS AISI 316L measured by conventional procedures, normally 8.0×10^3 kg m^{-3} [20].

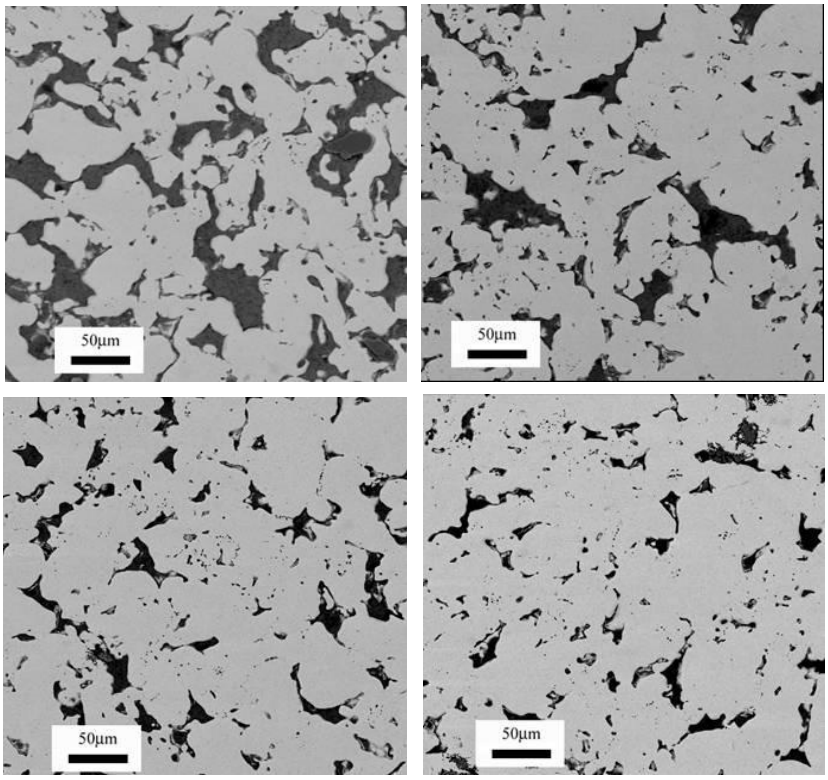

Figure 3. Evolution of the interconnected porosity for sintered SS AISI 316L as a function of compacting: (upper left frame) 400, 500, 600 MPa and (lower right frame) 700 MPa.

The sintered SS porosity distribution is shown in figure 3 for compacting pressures of 400, 500, 600 and 700 MPa, respectively. It may be seen that a significant change in the porosity has occurred, since the dark part starts from a large porous domain and, as the compacting rate increases, ends in a smaller one. Although it is not too obvious, those pictures may confirm the porosity behaviour presented in figure 2. This fact suggests that the use of high uniaxial pressure for compacting powder might induce a decrease in interconnected porosity. Thus, it may be expected that it could promote a better interaction between the particles by increasing the cross-section of the necks and the number of contacts. Reduction in porosity is intrinsically bound to the distinct processes that take place during the compacting and sintering procedures. Among the latter, there is the diffusion phenomenon of different elements that compose the material, which provides the mass transport and gives rise to a better homogeneity in terms of pore distribution. Furthermore, the marked phenomenon of diffusion induces neck formation between particles, a phenomenon related to the mass transport of the sintering process.

As previously commented, a standard SS AISI with the same OPC and the NATRC techniques was used for the whole set of measurements of thermal diffusivity, specific heat and thermal conductivity calculation. This reference sample was set to have nil porosity. Typically, the estimated absorbed power in the NATRC method was 12.75 mW for c_p and a differential temperature of 0.8 K was achieved during 40 s of illumination. An average $c_{\mathrm{p}} \sim 0.49 \times 10^3$ J kg^{-1} K^{-1} was found for the standard sample. This agrees with the value in the literature [20].

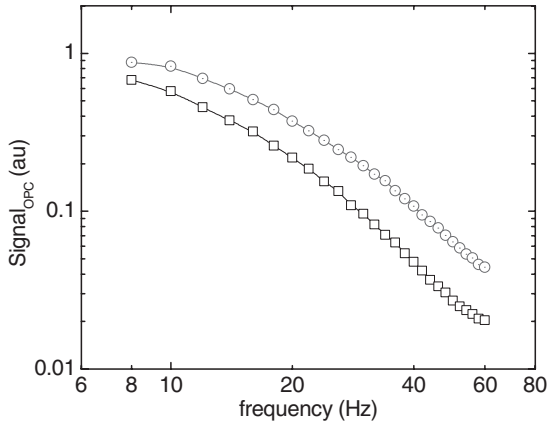

Figure 4. Log–log plot of a typical OPC signal. (□)—300 MPa and (⊙)—700 MPa.

Figure 4 shows a typical log–log plot of the OPC signal versus frequency for two representative samples, pressed at 300 and 700 MPa, respectively. As the OPC signal presents an exponential dependence, a linear behaviour in a semi-log plot, the parameters related to the thermal diffusivity may be obtained. In figure 5, the best fitting range occurred between 4 and 50 Hz. Actually, where $f > 50$ Hz, linear behaviour no longer exists. Dependence tails off the straight line, showing that there is another mechanism generating a photoacoustic signal. In fact, this is supposed to be related to either open pores or to the thermo-elastic effect [14, 15, 21] that may arise in the frequency range when the sample is over the quasithermally thick state. Since these effects are included in current research, they will not be discussed here. For the purpose of this paper, all fitting data were obtained by using the linear part of the OPC signal that assured the thermal diffusion as the dominant mechanism [15, 19]. Therefore, equation (2) may be used in data fitting. This hypothesis may be confirmed by comparing the frequency dependence of the signal for commercial SS foil. The latter should present only a straight line when the OPC signal is merely due to thermal diffusion mechanism. In fact figure 6 shows a linear dependence of the OPC signal obtained for a modulation frequency range up to nearly 200 Hz.

By using the relation $k = \rho c_p \alpha$, in which k is correlated with the compacting pressure, the thermal conductivity of the sintered material will be obtained. The thermal diffusivity results (α) reflect the same monotonic behaviour as those for the calculated thermal conductivity (k). Since the properties behave similarly between 10% (500 MPa) and 15% (300 MPa), the porosity produces either a small effect on the heat transfer properties or it forms a barrier for thermal transport in between particles. According to figure 2 and table 2, this limiting pressure is 495 MPa and refers to 10.5% of porosity. The behaviour has been obtained from data in figure 7. Note that the specific heat shown in figure 7 is quite linear and the dependence with porosity remains with thermal diffusivity and thermal conductivity.

At first glance, figure 7 brings out a similar behaviour when compared to the data in figure 2; for instance, an 'S-shaped' behaviour. In this case, the Boltzmann function $Bz(P)$ is still applicable even though the jump occurs in a very narrow range of porosity ($\sim$1% wide). Since α and k were fitted as a function of porosity a correlation between thermal properties and porosity could be obtained. The results are tabulated in table 3. Undertaking the same fitting as for ρ and $p\%$, the results show that the second derivative gives the inflection point for thermal diffusivity at $p\% \approx 8.02\%$, corresponding to $\alpha \approx 0.026 \times 10^{-4}$ m^2 s^{-1}. In the

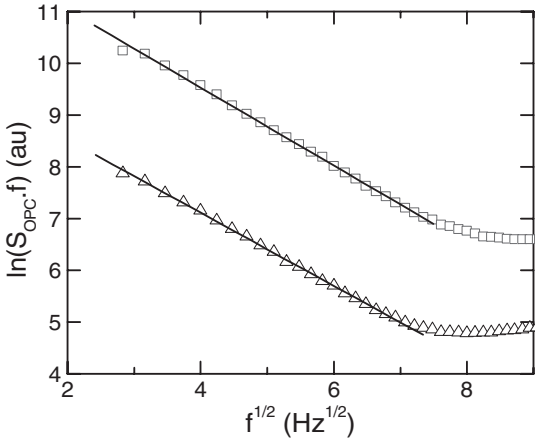

Figure 5. Linearized OPC fitting for two representative samples showing the linear range where the thermal diffusion mechanism is dominant ($f_{\max} \sim 50$ Hz). (△)—data for 300 MPa, fitted $\alpha = 0.021 \times 10^{-4}$ m^2 s^{-1} and (□)—700 MPa, fitted $\alpha = 0.032 \times 10^{-4}$ m^2 s^{-1}.

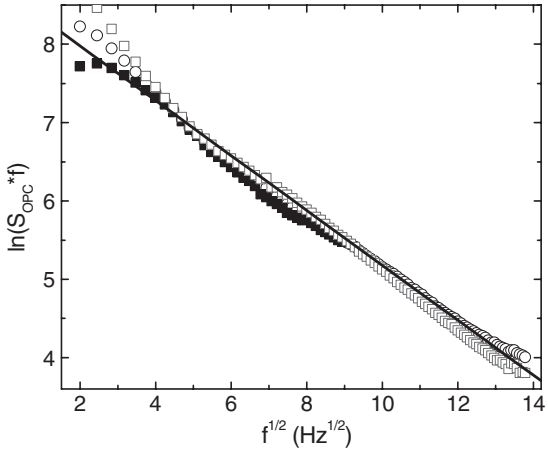

Figure 6. Linearized OPC fitting for a 560 μm thick SS foil illuminated with 500 mW at 514 nm. The thermal diffusion mechanism is dominant until $f_{\max} \sim 200$ Hz. The line is the average fitting giving $\alpha_{\text{avg}} = 0.035 \times 10^{-4}$ m^2 s^{-1} after three runs.

case of thermal conductivity, $p\% \approx 7.99\%$, this corresponds to $k \approx 0.10 \times 10^2$ W m^{-1} K^{-1}. Intrinsic porosity makes the analysis difficult because of the lack of specific models for thermal transport in a porous medium. As far as it is known, many of the thermal conductivity two-phase models are derived from empirical expressions mainly based on the Maxwell–Eucken relationship for a continuous solid matrix phase having a spherical dispersed phase. In the present discussion, the second phase is the porous one. It is important that a two-phase system produces an 'S-shaped' behaviour when thermal conductivity is plotted against the disperse phase content [22].

Now, let us analyse figure 7 from the right to the left in the porosity scaling. It may be seen that the thermal conductivity increases rapidly as the porosity decreases until it reaches 0.11×10^2 W m^{-1} K^{-1} (density $\sim 7.2 \times 10^3$ kg m^{-3} and porosity $\sim 8\%$); after this value (for

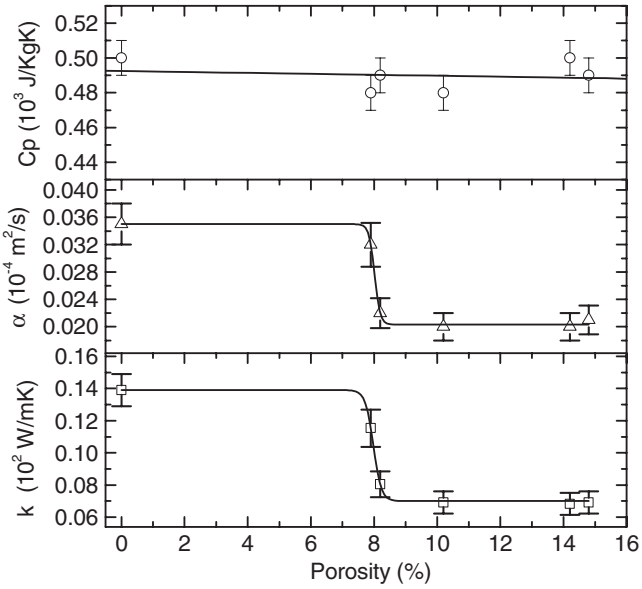

Figure 7. Results for measured values of specific heat and thermal diffusivity and comparison between calculated thermal conductivity and diffusivity with porosity. While the specific heat is linear there is a threshold for porosity near 8%, in which k suddenly increases reaching almost the value of the SS foil with nil porosity. (O)—specific heat, (△)—thermal diffusivity and (□)—thermal conductivity.

Table 3. Boltzmann analysis of thermal diffusivity (α) and thermal conductivity (k).

Boltzmann parameters	Diffusivity curve	Conductivity curve
I_s	$(0.035 \pm 0.003) \times 10^{-4}$ m^2 s^{-1}	$(0.14 \pm 0.01) \times 10^2$ W m^{-1} K^{-1}
F_s	$(0.020 \pm 0.001) \times 10^{-4}$ m^2 s^{-1}	$(0.07 \pm 0.01) \times 10^2$ W m^{-1} K^{-1}
H_s (porosity)	$(8.0 \pm 0.1)\%$	$(7.98 \pm 0.09)\%$
W	$(0.09 \pm 0.06)\%$	$(0.13 \pm 0.06)\%$

$\rho > 7.2 \times 10^3$ kg m^{-3}), it is expected to reach the value of the SS foil itself ($p = 0\%$ or $P \sim \infty$).

Previous works present models for porosity–thermal conductivity relations that emphasize that an exponential behaviour is expected for good conducting porous materials [23]. Many of these theoretical treatments use a first-order approximation to either a linear $k = k_0(1 - \gamma p)$, known as Loeb, modified for low porosity or an exponential form $k = k_0 \exp(-\eta p)$, or Hansen's model. In both proposals, p is porosity and the constants γ and η are related to pore structure and its distribution. Constants vary from $\gamma, \eta = 1$ to 2 for spherical pores or foams and $\gamma, \eta > 5$ for a solid with pores randomly distributed and sized [8].

In the present case, even though the thermal conductivity behaviour does not fit these models, it is possible to have insights about the pores' size and distribution by fitting both models to data. Using Hansen's approach, $\eta \sim 5.1$; from Loeb's model, $\gamma \sim 3.8$. Despite the poor fitting, the results suggest that the pores in the sample are more likely to be seen as randomly distributed and randomly sized. This agrees with the SEM results shown partially in the sequence in figure 3. In fact, the real mechanism of thermal transport of the SS

sintered should be developed in a different way. Since it is an almost porous free material, the theoretical model for an effective thermal transport should be considered, taking into account pore characteristics (pore size, geometry and distribution) and the ratio for the fractional volume of the solid phase.

In an attempt to understand the effect observed in the current thermal data, this problem may be discussed by taking a parallel view with respect to an electric conducting material. The porous system reflects a medium with two components, the electric insulating pores and the solid electric conducting phase. The sudden increase of thermal conductivity does not satisfy the two-phase model based on the effective medium [24, 25]. Walther and co-workers [4] recently proposed such an explanation. They observed this behaviour in a polymer doped by carbon particles, and proposed an additional transport mechanism in which the doping reaches a limiting concentration where an insulator–conducting transition takes place. In this condition, the density of the electrically conducting clusters exceeded the percolation threshold of the matrix. This behaviour seems to be that observed in the experimental data of the current SS 316L. Although there is no certainty whether a two-phase model is applied either to the pore phase or to the solid phase, figure 3 shows that the pores are isolated in a continuous solid matrix. In this case, for pressures over 500 MPa, the porosity tends to a saturating limit, as previously shown in figure 2. Reduction of porosity increased the density of particle contacts that probably exceeded the percolation threshold. It is believed that this condition provides a better contact for the powder particles and, therefore, facilitates thermal transport by improving contact in the powder chains. The thermal conductivity of the solid phase depends on the thermal conductivity of the particles that comprise the sintered material. Figure 7 seems to show that the solid phase thermal conductivity presents a cumulative interface thermal resistance in the transitional range. Estimates are possible if one considers $k \sim 0.13 \times 10^2$ W m^{-1} K^{-1} for $p < 9.0\%$ and $k \sim 0.07$ for $p > 9.0\%$. This difference amounts to about 0.06×10^2 W m^{-1} K^{-1} and is probably due to a two-phase coexistence in the range $p > 9\%$ which gives an effective value for thermal conductivity that is built up by both pore phase and solid phase. When $p < 9\%$, the solid-phase appears to be dominant.

Thus, a specific two-phase model that takes into account the solid phase thermal conductivity may be applied to this problem. Further theoretical investigations are needed in order to propose a two-phase model for the effective thermal conductivity of the porous medium that contains isolated pores in a continuous solid matrix.

5. Conclusion

Since the density presents a saturating behaviour, corresponding to 92% of SS AISI 316L, this material may be used as structural material. In addition, it has been evidenced that sintered SS AISI 316L presents a transition in the thermal conductivity for a very low porosity, of the order of 9%, when compacted at pressures over 500 MPa. According to the correlation between thermal properties, density and porosity, effects induced in the microstructure appear to be more pronounced only at high compacting rates, when the density of particle contact exceeds their percolation threshold. Posterior to this limit, a sudden increasing behaviour has been observed.

AISI 316L is an alloy with a specific composition, and thermal diffusion in such a porous material is influenced by the area of particle contact that is formed by the sintering process. A decrease in the porosity consequently leads the contact density in between the particles to increase. Besides, the gas phase in the sintered material decreases because of the decreasing porosity; this allows better thermal coupling for the particles once many necks are present after the sintering process. The proposal is that after a certain porosity limit the two-phase

behaviour becomes a single phase, a metallic phase, and the thermal conductivity goes toward the foil value quoted for the reference stainless steel.

In fact, as we address the discussion in the text, the mechanism should be something close to a two-phase model but in the porosity range over 10% of porosity. The lower value of the thermal conductivity supports this argument. On the other hand, if the porosity gets lower, and less than say 8%, a change in the behaviour comes up and the main mechanism is, in our opinion, mainly due to electronic processes. Moreover, we have the needs of a more perfect model that takes into account the porous geometry, size and distribution in a considered way in order to understand better how such a thermal transport takes place in sintered materials. This is left to people in the field that could be encouraged to assume such a challenge as well as for us.

Finally, the results evidenced the capacity of the open photoacoustic cell and the non-adiabatic thermal relaxation calorimetric methods to determine the absolute values of the thermal properties of sintered SS AISI 316L. The procedures of this current research may be useful in the study of other porous materials.

Acknowledgments

The authors would like to thank Dr C E Costa for the SEM facilities and Dr H G Walther for fruitful discussion. The Brazilian agencies CNPq, Capes and Fundação Araucária supported this research.

References

[1] Lenel F V 1980 *Powder Metallurgy: Principles and Applications* (Princeton, NJ: Metal Powder Industries Federation)
[2] Parrott J E and Stuckes A D 1975 *Thermal Conductivity of Solids* (New York: Methuen)
[3] Hasselman D P H, Venkateswaran A, Yu M and Tawil H 1991 *J. Mater. Sci. Lett.* **10** 1037
[4] Walther H G, Kitzing T, Bozoki Z, Liakhou G L and Paoloni S 1999 *J. Appl. Phys.* **85** 7540
[5] Surnev S, Lepkova D and Yoleva A 1991 *Mater. Sci. Eng.* B **10** 35
[6] Agari Y, Ueda A and Nagai S 1991 *J. Appl. Polym. Sci.* **43** 1117
[7] Lee R-R 1991 *J. Am. Ceram. Soc.* **74** 2242
[8] Enloe J H, Rice R W, Lau J W, Kumar R and Lee S Y 1991 *J. Am. Ceram. Soc.* **74** 2214
[9] Woodside W and Messmer J H 1961 *J. Appl. Phys.* **32** 1688
[10] Tam A C 1986 *Rev. Mod. Phys.* **58** 381
[11] Mandelis A (ed) 1992 *Progress in Photothermal and Photoacoustic Science and Technology* vol 1 (New York: Elsevier)
[12] Vargas H and Miranda L C M 1988 *Phys. Rep.* **161** 43
[13] Pan G and Mandelis A 1998 *Rev. Sci. Instrum.* **69** 2918
[14] da Silva M D, Bandeira I N and Miranda L C M 1987 *J. Phys. E. Sci. Instrum.* **20** 1476
[15] Balderas-López J A and Mandelis A 2000 *Rev. Sci. Instrum.* **88** 6815
[16] Calderón A, Alvarado-Gil J J, Gurevich Yu G, Cruz-Orea A, Delgadillo I, Vargas H and Miranda L C M 1997 *Phys. Rev. Lett.* **79** 5022
[17] Medina A N, Caldeira A M F, Bento A C, Baesso M L, Sampaio J A, Catunda T and Gandra F G 2002 *J. Non-Cryst. Solids* **304** 299
[18] Bachmann R, Schwall R E, Thomas H U, Zubeck R B, King C N, Kirsch H C, DiSalvo F J, Geballe T H, Lee K N, Howard R E and Greene R L 1972 *Rev. Sci. Instrum.* **43** 205
[19] Rosencwaig A and Gersho A 1976 *J. Appl. Phys.* **47** 64
[20] Almond D P and Patel P M 1996 *Photothermal Science and Techniques* (London: Chapman and Hall) pp 16–7
[21] McDonald F A and Wetzel G W Jr 1988 *Physical Acoustic, Principles and Methods* vol XVIII, ed W P Mason and R N Thurston (San Diego, CA: Academic) chapter 4, pp 167–277
[22] Kingery W D 1975 *Introduction to Ceramics* (New York: Wiley) pp 499–509
[23] Gibkes J, Bein B, Krüger D and Pelzl J 1993 *Carbon* **31** 801
[24] Velinov T, Bransalov K and Mihovski M 1993 *Meas. Sci. Technol.* **4** 1266
[25] Singh K J, Singh R and Chaudhary D R 1998 *J. Phys. D: Appl. Phys.* **31** 1681